Protein NMR Spectroscopy

DOI: 10.1002/anie.201301215

NMR Spectroscopy of Soluble Protein Complexes at One Mega-Dalton and Beyond**

*Andi Mainz, Tomasz L. Religa, Remco Sprangers, Rasmus Linser, Lewis E. Kay, and Bernd Reif**

Solution-state nuclear magnetic resonance (NMR) spectroscopy is a very successful method to characterize the structure and dynamics of biomolecules in solution.[1,2] However, resonance lines broaden significantly with increasing molecular weight, simultaneously affecting sensitivity and resolution. This broadening is due to long rotational tumbling correlation times τ_c, which enhance transverse relaxation.[3] Deleterious relaxation effects can be partially avoided by the use of transverse relaxation-optimized spectroscopy (TROSY), which is based on mutual cancellation of different relaxation pathways and which allows the selection of slowly relaxing multiplet components.[4,5] TROSY-type techniques have thus enabled the characterization of supramolecular assemblies like GroEL-GroES,[6] p53/Hsp90,[7] the ATPase motor SecA,[8] ClpP,[9] or the 20S proteasome.[10,11] However, even at very high magnetic fields, low molecular tumbling rates limit the applicability of solution-state NMR. In particular, the assignment of backbone resonances becomes increasingly difficult for protein complexes beyond 80 kDa. Typically, methyl-based experiments are carried out for very large systems, as contributions from overall tumbling are reduced owing to the fast three-fold rotation of the methyl group.[5]

In magic-angle spinning (MAS) solid-state NMR, immobilized samples are spun rapidly in a cylindrical rotor, which is inclined at an angle Θ_{MA} of 54.74° relative to the magnetic field of the NMR spectrometer.[12] MAS yields resonance line narrowing by refocusing coherent anisotropic interactions, such as the dipolar coupling and the chemical shift anisotropy. Notably, the resonance line width in MAS solid-state NMR is independent of the protein molecular weight. However, rigid solids are required, entailing elaborate precipitation or crystallization procedures for biological macromolecules in a potentially non-native environment. We have shown recently that protein complexes, which are filled as solutions into the NMR rotor, can be investigated by MAS NMR.[13,14] Originally, we coined this approach FROSTY (freezing rotational diffusion of protein solutions at low temperature and high viscosity) MAS NMR, implying that rotational reorientation of the protein is impeded in the MAS experiment.[13] We speculated that high protein concentration results in molecular crowding, which would facilitate solid-state NMR approaches.[13] Bertini et al. have further elucidated that strong centrifugal forces during MAS lead to reversible protein sedimentation, and named these experiments SedNMR.[15] The dense packing of protein molecules at the inner wall of the MAS rotor thus impairs molecular tumbling, which has been reported to occur on the low microsecond timescale in the absence of MAS.[16] We demonstrate herein that the FROSTY MAS approach greatly simplifies conventional solid-state NMR sample preparation, and that it enables proton-detected backbone-based NMR experiments for very large protein assemblies under native conditions, thereby overcoming the molecular weight limit of traditional solution-state NMR.

We focus here on the proteasome degradation machinery, which is essential for cellular protein homeostasis and viability.[17] The 20S proteasome of *Thermoplasma acidophi-*

[*] Dr. A. Mainz, Prof. Dr. B. Reif
Munich Center for Integrated Protein Science (CIPS-M) at the Department Chemie, Technische Universität München (TUM)
Lichtenbergstrasse 4, 85747 Garching (Germany)
E-mail: reif@tum.de
Dr. A. Mainz, Prof. Dr. B. Reif
Helmholtz-Zentrum München (HMGU)
Deutsches Forschungszentrum für Gesundheit und Umwelt
Neuherberg (Germany)
Dr. A. Mainz, Prof. Dr. B. Reif
Leibniz-Institut für Molekulare Pharmakologie (FMP)
Berlin (Germany)
Prof. Dr. T. L. Religa, Prof. Dr. L. E. Kay
University of Toronto, Department of Medical Genetics and Microbiology (Canada)
Prof. Dr. L. E. Kay
Program in Molecular Structure and Function
Hospital for Sick Children, Toronto (Canada)
Dr. R. Sprangers
Max Planck-Institute for Developmental Biology
Tübingen (Germany)
Dr. R. Linser
Harvard Medical School, Department of Biological Chemistry and Molecular Pharmacology
Boston (USA)
Dr. R. Linser
School of Chemistry, UNSW, Sydney (Australia)

[**] This work was performed in the framework of SFB-1035/Project-B07 (German Research Foundation, DFG). We acknowledge support by the Leibniz-Gemeinschaft, the Helmholtz-Gemeinschaft, and the Deutsche Forschungsgemeinschaft (Grants Re1435). We are also grateful to the Center for Integrated Protein Science Munich (CIPS-M) for financial support (A.M., B.R.). This work was further supported by the Max Planck Society (R.S.) and by a grant from the Canadian Institutes of Health Research (CIHR) (T.L.R., L.E.K.). L.E.K. holds a Canada Research Chair in Biochemistry. R.L. was supported by an Australian Research Council Discovery Early Career Research Award.

© 2013 Wiley-VCH Verlag GmbH & Co. KGaA, Weinheim

lum is ideally suited to demonstrate the FROSTY concept because of its modular assembly. The α-subunit (26 kDa) alone forms a double heptameric ring structure $\alpha_7\alpha_7$ (360 kDa) in solution (Figure 1). The native full proteasome core particle $\alpha_7\beta_7\beta_7\alpha_7$ (670 kDa) assembles upon addition of the β-subunit into a four-ring barrel-like structure (Figure 1).[18,19] The 1.1 MDa 11S-$\alpha_7\beta_7\beta_7\alpha_7$-11S complex is formed through interaction with two heptameric 11S activator lids from *Trypanosoma brucei* on both sides of the $\alpha_7\beta_7\beta_7\alpha_7$ barrel (Figure 1).[18,19] It is noteworthy that only the α-subunit was isotopically enriched with ^{13}C and ^{15}N in our NMR experiments. Whilst observing exclusively the NMR-active α-subunit, the molecular weight of the respective proteasome assembly was successively increased by adding the NMR-invisible β-subunit and 11S activator.

Highly concentrated protein solutions were directly used for MAS NMR experiments without any further treatment. Despite its molecular weight, the 1.1 MDa 11S-$\alpha_7\beta_7\beta_7\alpha_7$-11S complex yields well-resolved 2D ^1H–^{15}N correlation spectra with line widths on the order of 40 Hz (^1H) and 20 Hz (^{15}N), respectively (Figure 2 A). This resolution is comparable to that observed for crystalline model systems.[20] Proton-detected experiments were carried out as the sensitivity in NMR spectroscopy is proportional to $\gamma^{3/2}$, with γ being the gyromagnetic ratio of the detected nucleus ($\gamma_{1H} \cong 4\gamma_{13C} \cong 10\gamma_{15N}$). For this purpose, we employed protea-

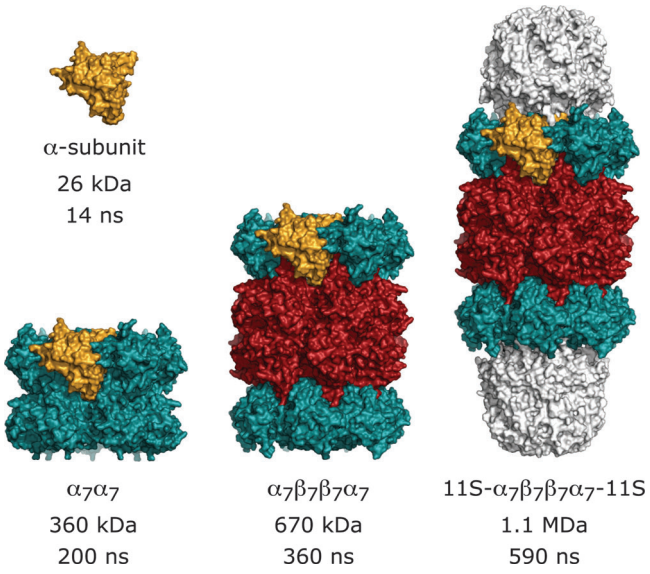

Figure 1. The modular architecture of the archaeal 20S proteasome. Side view of different proteasome species of *Thermoplasma acidophilum*[18] and *Trypanosoma brucei*[19] with their molecular weight and rotational correlation time τ_c (calculated for 30 °C). The heptameric rings of the α-, β-, and 11S-subunits are colored in green, red, and white, respectively. One α-subunit is highlighted in orange in each case. In the NMR experiments, only the α-subunits were isotopically enriched.

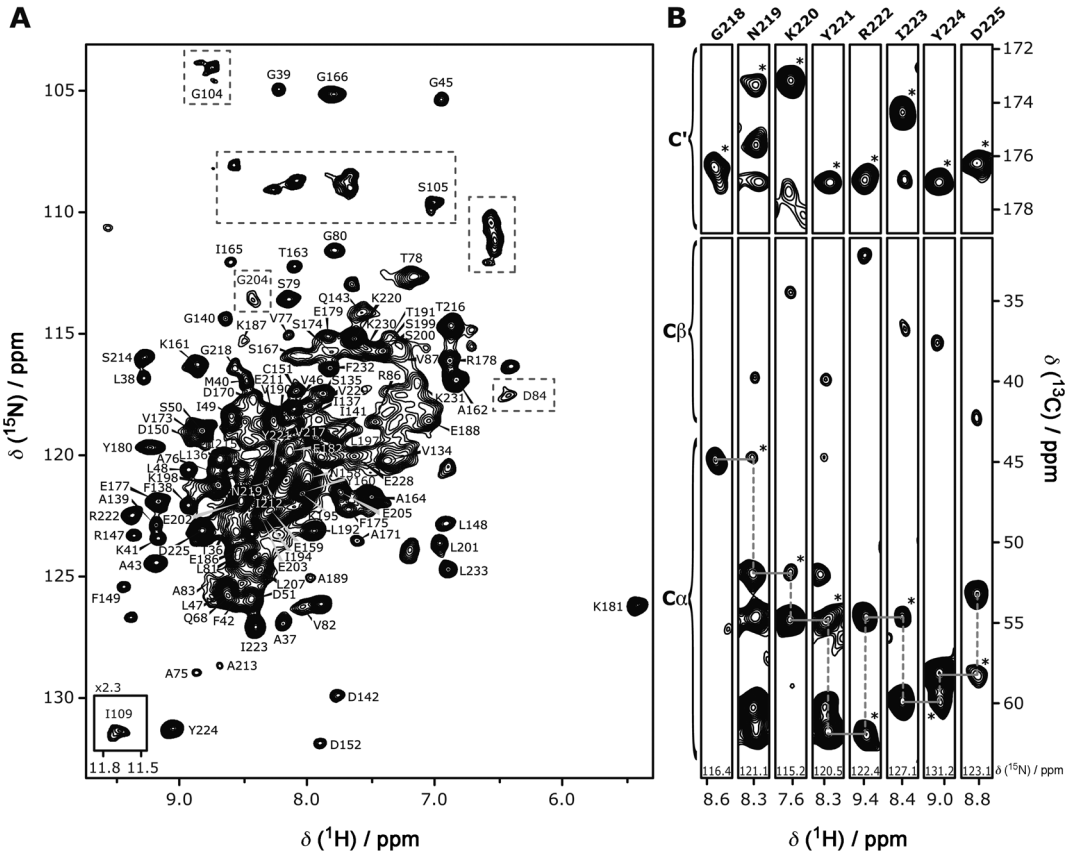

Figure 2. Resonance assignment of the proteasome α-subunit within the 1.1 MDa 11S-$\alpha_7\beta_7\beta_7\alpha_7$-11S complex by FROSTY MAS NMR. A) 2D ^1H–^{15}N correlation spectrum with assignments.[30] Note that resonances in dashed boxes are drawn at lower contour levels (2.3×) for better visualization. I109 is shown in the inset (left bottom). B) 2D strips are extracted from 3D hCOhNH and hCAhNH spectra (pulse sequence adapted from Ref. [24]; see the Supporting Information, Figure S5), illustrating Cα, Cβ, and carbonyl resonances for residues G218–D225. Inter-residual contacts to the preceding residue are marked with asterisks.

 © 2013 Wiley-VCH Verlag GmbH & Co. KGaA, Weinheim

some samples sparsely protonated (ca. 20%) at amide sites and fully deuterated at non-exchangeable groups.[20] In solution-state NMR, deuteration is required to suppress undesired relaxation pathways.[21] In the solid-state, deuteration reduces the strong ^{1}H–^{1}H dipolar coupling network and facilitates line narrowing by MAS. Moreover, the paramagnetic agent Cu^{II}-EDTA was added to the samples[22,23] to speed up data acquisition by a factor of more than 10 (see the Supporting Information).

We find that the signal-to-noise ratio improves significantly with increasing molecular weight of the proteasome complex (Figure 3). We note that all three proteasome assemblies shown in Figure 3 are expected to sediment completely (>97%) at the employed rotation frequency of 22 kHz (see the Supporting Information). Therefore, the sensitivity increase seems to be ascribed to reduced rotational mobility of the larger assemblies in the sedimented state, which is possibly due to a more pronounced self-crowding. The resolution in the ^{1}H and ^{15}N dimensions also improves with higher molecular weight (Figure 3), which may be attributed to the same effect. Our observations thus imply that high molecular weights improve the spectral resolution and sensitivity in FROSTY MAS experiments. However, we cannot rule out that differential internal dynamics of the three complexes may also contribute to these observations.

2D ^{1}H–^{13}C correlation spectra using deuterated $\alpha_7\alpha_7$ with specifically protonated methyl groups of isoleucines, leucines, and valines (see the Supporting Information) show a similar signal pattern as observed by solution-state NMR, however with decreased resolution (Supporting Information, Figure S1). Backbone resonances benefit more from the MAS approach in comparison to the fast rotating methyl groups, which have reduced transverse relaxation rates in solution-state NMR.[5]

The effect of molecular weight on spectral resolution and sensitivity is readily appreciated in ^{13}C-detected experiments. Even though the concentration of the core particle $\alpha_7\beta_7\beta_7\alpha_7$ (2.3 mM α-subunit concentration) is smaller in comparison to

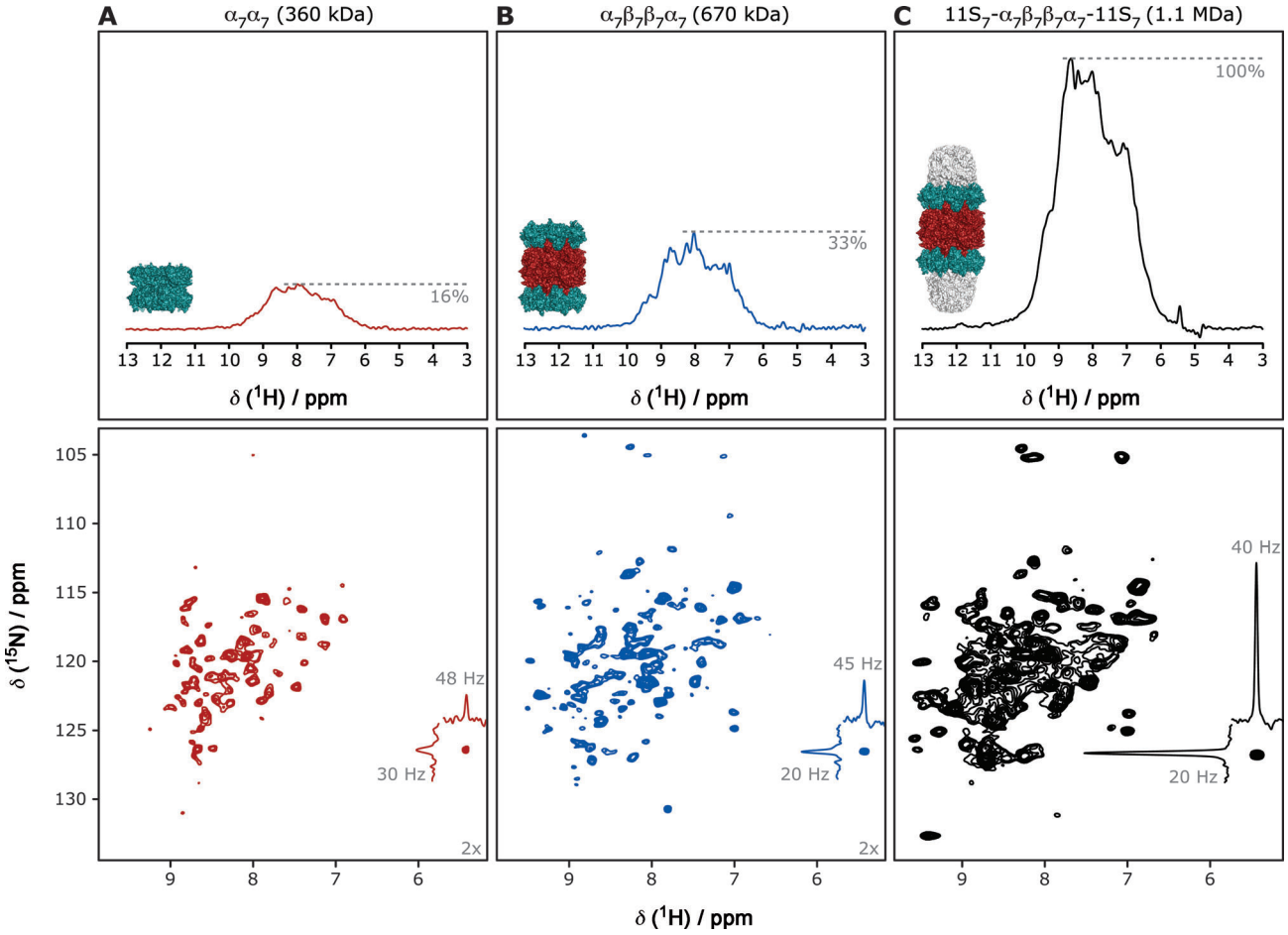

Figure 3. Proton-detected MAS experiments and the effect of increasing molecular weight. 2D ^{1}H–^{15}N correlation spectra (bottom) based on cross-polarization (CP) and the corresponding 1D version (top) of the 360 kDa $\alpha_7\alpha_7$ (A), the 670 kDa $\alpha_7\beta_7\beta_7\alpha_7$ (B,) and the 1.1 MDa 11S-$\alpha_7\beta_7\beta_7\alpha_7$-11S complex (C). The spectra were recorded at 0°C and with 22 kHz MAS. Acquisition and processing parameters were identical. The employed concentration of the NMR-active α-subunit amounted to 3.3 mM ($\alpha_7\alpha_7$), 1.9 mM ($\alpha_7\beta_7\beta_7\alpha_7$), and 3.0 mM (11S-$\alpha_7\beta_7\beta_7\alpha_7$-11S), respectively. The signal intensities of ^{15}N-filtered ^{1}H-1D spectra are normalized to account for the different concentrations of the α-subunit. Note that contour levels of 2D spectra are drawn at 8σ (A, B) and 16σ (C) from the noise floor. 1D projections of the K181 cross-peaks as well as the corresponding ^{1}H and ^{15}N line widths at half-height are given (right bottom). The average ^{1}H and ^{15}N line widths (10 representative cross-peaks) yield 68±18 Hz and 35±7 Hz ($\alpha_7\alpha_7$), 54±11 Hz and 24±4 Hz ($\alpha_7\beta_7\beta_7\alpha_7$), and 48±8 Hz and 22±1 Hz (11S-$\alpha_7\beta_7\beta_7\alpha_7$-11S), respectively.

© 2013 Wiley-VCH Verlag GmbH & Co. KGaA, Weinheim

the $\alpha_7\alpha_7$ double ring (3.5 mM α-subunit concentration), more resonances are observed in the 2D ^{13}C–^{13}C correlation spectrum (Figure 4A,B).

Differences in the cross-polarization (CP)[25,26] transfer behavior indicate increased exchange dynamics for the smaller $\alpha_7\alpha_7$ (Figure 4C). Disregarding internal motions, this may arise from residual overall reorientation of $\alpha_7\alpha_7$ in the MAS-induced sediment, thereby compromising the sensitivity and resolution in the spectra. To probe whether the molecular-weight-dependent increase in FROSTY signal intensities is due to ns–μs timescale motions, we recorded TROSY-based ^{1}H–^{15}N correlation spectra for perdeuterated 11S-$\alpha_7\beta_7\beta_7\alpha_7$-11S. For residues undergoing motion on this timescale, such experiments have shown improved transfer properties in solid samples.[27] However, for 11S-$\alpha_7\beta_7\beta_7\alpha_7$-11S application of TROSY did not improve the spectral quality under FROSTY conditions (Supporting Information, Figure S2B,C). Furthermore, only six additional cross-peaks could be observed exclusively in scalar coupling-based experiments (Supporting Information, Figure S2A). We can therefore exclude fast/intermediate timescale motion as playing a major role in the experiments.

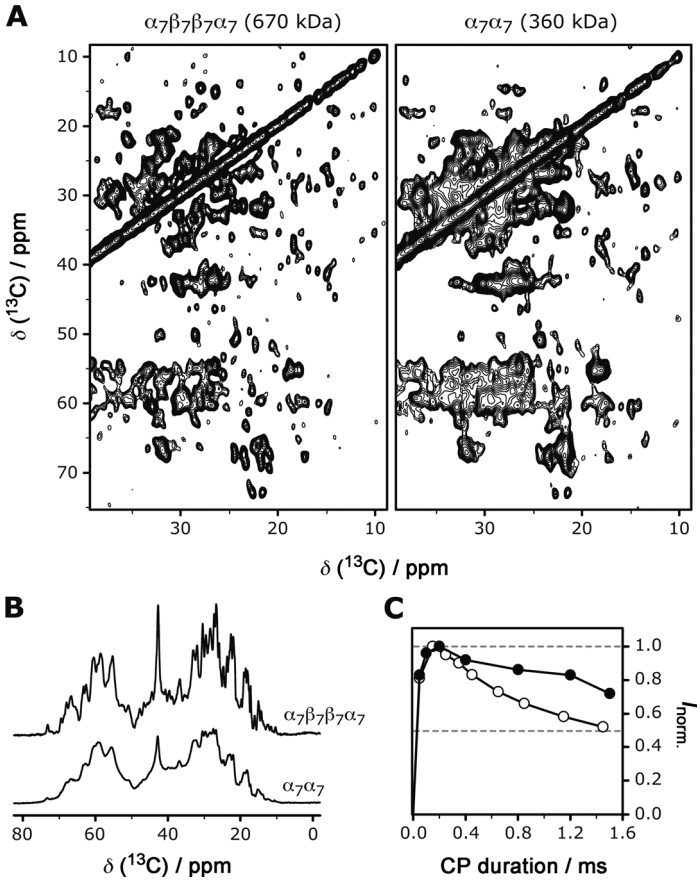

Figure 4. Improvement in spectral resolution and sensitivity with larger molecular weight, shown for $\alpha_7\alpha_7$ (360 kDa) and $\alpha_7\beta_7\beta_7\alpha_7$ (670 kDa). A) Aliphatic region of 2D ^{13}C–^{13}C correlation spectra under identical experimental conditions, except that the spectrum of $\alpha_7\alpha_7$ was recorded with twice the number of scans. The monomer concentration of the α-subunit amounted to 3.5 mM ($\alpha_7\alpha_7$) and 2.3 mM ($\alpha_7\beta_7\beta_7\alpha_7$), respectively. Both spectra are drawn at 4σ with respect to the noise to allow for proper comparison. B) Aliphatic region of 1D ^{13}C spectra with the signal intensities corrected for the different concentrations. The spectra were acquired and processed identically. C) CP build-up curves are shown for the bulk aliphatic region of $\alpha_7\alpha_7$ (○) and $\alpha_7\beta_7\beta_7\alpha_7$ (●).

Superposition of the CP-based ^{1}H–^{15}N correlation spectrum of 11S-$\alpha_7\beta_7\beta_7\alpha_7$-11S with the solution-state ^{1}H–^{15}N TROSY spectrum of the single ring construct α_7 (180 kDa)[11] illustrates the high degree of similarity between the two sample preparations (Supporting Information, Figure S3). Peak picking yields approximately 130 cross-peaks for 11S-$\alpha_7\beta_7\beta_7\alpha_7$-11S. For the α_7 construct, 145 amide signals have been assigned for the 233-residue α-subunit.[11] In both cases, resonances are missing because of chemical exchange broadening. For 11S-$\alpha_7\beta_7\beta_7\alpha_7$-11S, an increase in temperature from 0 °C to 30 °C results in significant line-narrowing for several resonances (for example, I109, G166, Y224) owing to conformational averaging (Supporting Information, Figure S4). This is in contrast to the general trend that low temperatures yield higher signal intensities in dipolar-based FROSTY MAS experiments.

For assignment of 11S-$\alpha_7\beta_7\beta_7\alpha_7$-11S, long-range CP steps were employed to transfer the initial ^{1}H magnetization directly to the nearby ^{13}C nuclei, namely Cα and C′ (Supporting Information, Figure S5). Strips of the 3D hCAhNH and hCOhNH experiments are shown in Figure 2B (see the Supporting Information, Figure S5C for signal-to-noise ratios). These experiments are the dipolar analogues of the solution-state HNCA and HNCO experiments. Analysis of the spectra yields backbone resonance assignments for 108 out of 227 non-proline residues (Figure 2A).[30] Inter-residual contacts are mainly observed in the hCAhNH spectrum and enable sequential assignment of the protein backbone (Figure 2B). Observation of intra-residual Cβ correlations in hCAhNH experiments allows confirmation of the identity of individual residues (Figure 2B). In future studies, ^{13}C–^{13}C mixing will provide further side-chain information. Assignments were assisted and validated by comparison to the solution-state resonance assignment of α_7.[11]

The majority of non-observable residues can be found in the regions M1-S35, K52-V74, L88-Y103, and E110-G133 (Figure 5A). These regions include the N-terminal gate and the α-annulus, which occlude the entrance for substrates into the lumen of the proteasome, as well as the interaction site with the β-subunit (Figure 5B). Similar regions were invisible in solution-state NMR studies of the isolated α_7 ring owing to internal motions on the millisecond timescale.[10,11] Even though resonances of interfacial residues show significant chemical exchange broadening, interactions between the different subunits can be mapped by analysis of several chemical shift perturbations. Binding of the 11S activator to $\alpha_7\beta_7\beta_7\alpha_7$ induces chemical shift changes in particular for residues D152, I165, and G166, which are located close to the 11S activator binding site (Figure 5C,D). Furthermore, the analysis of ^{13}C chemical shifts allows prediction of secondary structure elements for

 © 2013 Wiley-VCH Verlag GmbH & Co. KGaA, Weinheim

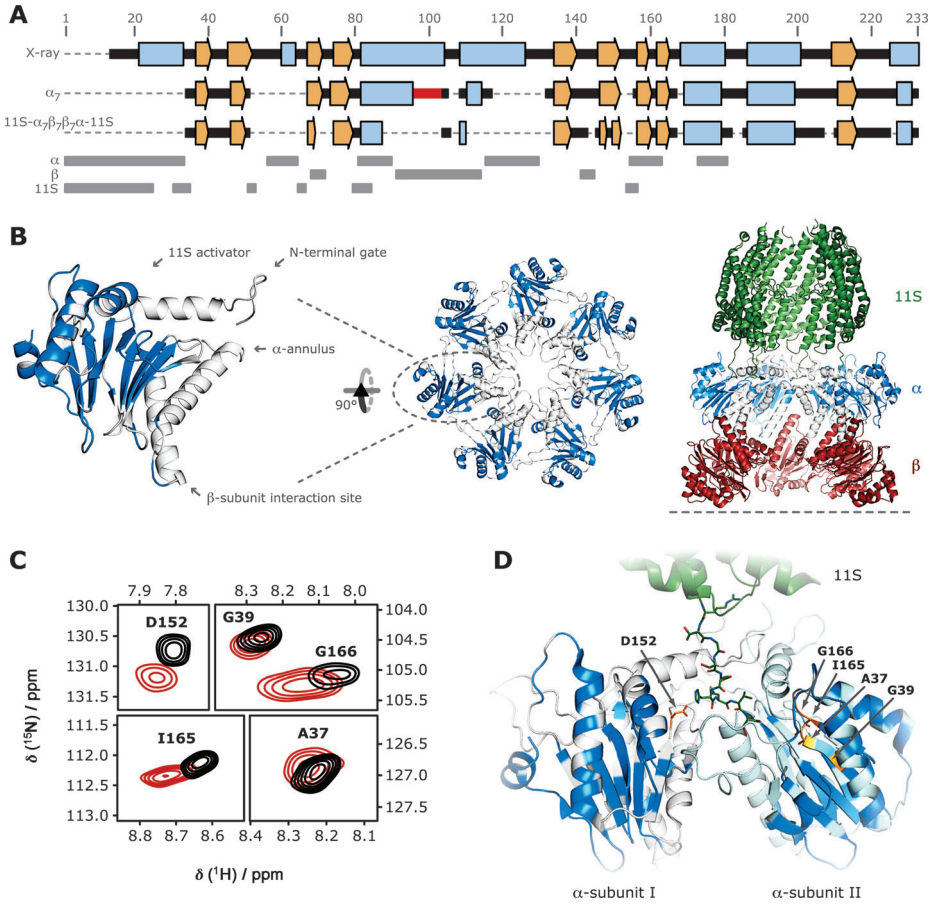

Figure 5. Intermolecular contacts in the proteasome assemblies. A) The secondary structure of the proteasome α-subunit as observed by X-ray crystallography is depicted on top.[19] The results from ^{13}C chemical shift analysis of TROSY- and FROSTY-observable residues of α_7[11] and 11S-$\alpha_7\beta_7\beta_7\alpha_7$-11S, respectively, are illustrated below. Secondary structure elements are represented in blue (α-helices), orange (β-strands), and black (other). Dashed lines correspond to not-assigned residues (ca. 20 cross-peaks) or non-observable residues. The sequence deletion in the α_7 construct, preventing association of two heptameric rings, is highlighted in red.[11] Regions within the α-subunit that are involved in intermolecular interactions with the α-subunit itself, the β-subunit, and the 11S activator are indicated on the bottom (gray bars). B) Residues that are assigned by FROSTY MAS NMR in the context of 11S-$\alpha_7\beta_7\beta_7\alpha_7$-11S are highlighted in blue. The N-terminal gate and the α-annulus as well as the interaction sites with the β-subunit (red) and the 11S activator (green) are indicated. The front half of the complex is omitted for better visualization (right). C) Sections of 2D ^1H–^{15}N correlation spectra of $\alpha_7\beta_7\beta_7\alpha_7$ (black) and 11S-$\alpha_7\beta_7\beta_7\alpha_7$-11S (red), showing chemical shift perturbations upon binding of the 11S activator. The corresponding residues are labeled and highlighted in orange in (D), showing the interface between the 11S activator (green) and two α-subunits (white and cyan).[19]

the α-subunit. Figure 5A shows the secondary structural elements as obtained for α_7[11] and 11S-$\alpha_7\beta_7\beta_7\alpha_7$-11S. Both predictions are very similar and in good agreement with the X-ray structure.[19]

The FROSTY MAS approach in combination with protein deuteration, proton detection, and paramagnetic relaxation enhancement has enabled us to observe and to assign backbone resonances of the α-subunit within the megadalton 11S-$\alpha_7\beta_7\beta_7\alpha_7$-11S proteasome complex. Sequential assignments are thus feasible for protein complexes beyond the molecular weight limit imposed by molecular tumbling in traditional solution-state NMR. Furthermore, we were able to extract consistent secondary structure information as well as to observe inter-subunit contacts within the assembly. In contrast to what is expected in conventional solution-state NMR, we find that the spectral quality improves with increasing molecular weight. Protein immobilization required for MAS solid-state NMR is induced by the MAS technique itself without any further sample manipulation.[13,15] As shown recently, the sensitivity can be improved by direct ultracentrifugation into the MAS rotor.[28,29] The approach can be easily transferred to other components of the proteasome, thereby enabling the analysis of substrate entrance and processing, as well as to other large protein assemblies. This technique thus opens new perspectives for the investigation of structure and dynamics of multi-component supramolecular machines at the atomic level.

Received: February 11, 2013
Revised: April 30, 2013
Published online: July 19, 2013

Keywords: magic-angle spinning · molecular weight limit · NMR spectroscopy · proteins · sedimentation

[1] K. Wüthrich, *NMR of Proteins and Nucleic Acids*, Wiley, New York, **1986**.
[2] A. G. Palmer, J. Williams, A. McDermott, *J. Phys. Chem.* **1996**, *100*, 13293–13310.
[3] J. Cavanagh, W. J. Fairbrother, A. G. Palmer III, N. J. Skelton, M. Rance, *Protein NMR Spectroscopy, Principles and Practice, 2nd ed.*, Academic Press, San Diego, **2006**.
[4] K. Pervushin, R. Riek, G. Wider, K. Wüthrich, *Proc. Natl. Acad. Sci. USA* **1997**, *94*, 12366–12371.
[5] V. Tugarinov, P. M. Hwang, J. E. Ollerenshaw, L. E. Kay, *J. Am. Chem. Soc.* **2003**, *125*, 10420–10428.
[6] J. Fiaux, E. B. Bertelsen, A. L. Horwich, K. Wüthrich, *Nature* **2002**, *418*, 207–211.
[7] S. Rudiger, S. M. V. Freund, D. B. Veprintsev, A. R. Fersht, *Proc. Natl. Acad. Sci. USA* **2002**, *99*, 11085–11090.
[8] I. Gelis, A. M. J. J. Bonvin, D. Keramisanou, M. Koukaki, G. Gouridis, S. Karamanou, A. Economou, C. G. Kalodimos, *Cell* **2007**, *131*, 756–769.
[9] R. Sprangers, A. Gribun, P. M. Hwang, W. A. Houry, L. E. Kay, *Proc. Natl. Acad. Sci. USA* **2005**, *102*, 16678–16683.
[10] R. Sprangers, L. E. Kay, *Nature* **2007**, *445*, 618–622.
[11] R. Sprangers, X. Li, X. Mao, J. L. Rubinstein, A. D. Schimmer, L. E. Kay, *Biochemistry* **2008**, *47*, 6727–6734.

© 2013 Wiley-VCH Verlag GmbH & Co. KGaA, Weinheim

[12] E. R. Andrew, A. Bradbury, R. G. Eades, *Nature* **1958**, *182*, 1659.
[13] A. Mainz, S. Jehle, B. J. van Rossum, H. Oschkinat, B. Reif, *J. Am. Chem. Soc.* **2009**, *131*, 15968 – 15969.
[14] A. Mainz, B. Bardiaux, F. Kuppler, G. Multhaup, I. C. Felli, R. Pierattelli, B. Reif, *J. Biol. Chem.* **2012**, *287*, 1128 – 1138.
[15] I. Bertini, C. Luchinat, G. Parigi, E. Ravera, B. Reif, P. Turano, *Proc. Natl. Acad. Sci. USA* **2011**, *108*, 10396 – 10399.
[16] E. Ravera, G. Parigi, A. Mainz, T. L. Religa, B. Reif, C. Luchinat, *J. Phys. Chem. B* **2013**, *117*, 3548 – 3553.
[17] W. Baumeister, J. Walz, F. Zühl, E. Seemüller, *Cell* **1998**, *92*, 367 – 380.
[18] J. Löwe, D. Stock, B. Jap, P. Zwickl, W. Baumeister, R. Huber, *Science* **1995**, *268*, 533 – 539.
[19] A. Förster, E. I. Masters, F. G. Whitby, H. Robinson, C. P. Hill, *Mol. Cell* **2005**, *18*, 589 – 599.
[20] V. Chevelkov, K. Rehbein, A. Diehl, B. Reif, *Angew. Chem.* **2006**, *118*, 3963 – 3966; *Angew. Chem. Int. Ed.* **2006**, *45*, 3878 – 3881.
[21] D. Nietlispach, R. T. Clowes, R. W. Broadhurst, Y. Ito, J. Keeler, M. Kelly, J. Ashurst, H. Oschkinat, P. J. Domaille, E. D. Laue, *J. Am. Chem. Soc.* **1996**, *118*, 407 – 415.
[22] R. Linser, V. Chevelkov, A. Diehl, B. Reif, *J. Magn. Reson.* **2007**, *189*, 209 – 216.
[23] N. P. Wickramasinghe, S. Parthasarathy, C. R. Jones, C. Bhardwaj, F. Long, M. Kotecha, S. Mehboob, L. W.-M. Fung, J. Past, A. Samoson, Y. Ishii, *Nat. Methods* **2009**, *6*, 215 – 218.
[24] R. Linser, *J. Biomol. NMR* **2012**, *52*, 151 – 158.
[25] S. R. Hartmann, E. L. Hahn, *Phys. Rev.* **1962**, *128*, 2042 – 2053.
[26] A. Pines, M. G. Gibby, J. S. Waugh, *J. Chem. Phys.* **1973**, *59*, 569 – 590.
[27] R. Linser, U. Fink, B. Reif, *J. Am. Chem. Soc.* **2010**, *132*, 8891 – 8893.
[28] I. Bertini, F. Engelke, C. Luchinat, G. Parigi, E. Ravera, C. Rosa, P. Turano, *Phys. Chem. Chem. Phys.* **2012**, *14*, 439 – 447.
[29] C. Gardiennet, A. K. Schütz, A. Hunkeler, B. Kunert, L. Terradot, A. Böckmann, B. H. Meier, *Angew. Chem.* **2012**, *124*, 7977 – 7980; *Angew. Chem. Int. Ed.* **2012**, *51*, 7855 – 7858.
[30] The chemical shift assignment for the α-subunit in 11S-$\alpha_7\beta_7\beta_7\alpha_7$-11S has been deposited in the BMRB under accession number 19194.

 © 2013 Wiley-VCH Verlag GmbH & Co. KGaA, Weinheim